Orbital-level Engineering of Bonding Networks to modulate Halogen Migration in Lead-Free Double Perovskites

Qianglong Fang[1,3], Mingao Hu[1,3], Xinying Gao[1], Yilei Wu[1], Qun Ji[1], Ming-Gang Ju[1]*, Jinlan Wang[1,2]

[1]Key Laboratory of Quantum Materials and Devices of Ministry of Education, School of Physics, Southeast University, Nanjing 211189, China.

[2] Suzhou Laboratory, Suzhou, China.

[3]These authors contributed equally: Qianglong Fang, Mingao Hu.

*Corresponding author.
E-mail addresses: juming@seu.edu.cn

Supplementary Notes

Note S1 Criteria for determining the formability of HDPs.

Before performing machine learning predictions, we pre-screened the stability of halide double perovskite $A_2B_IB_{III}X_6$ by evaluating three widely used geometric stability descriptors: Goldschmidt's tolerance factor (t), the octahedral factor (μ), and the tolerance factor (τ), t and u were calculated as[1]:

$$t = \frac{r_A + r_X}{\sqrt{2\,(r_B + r_X)}}$$

$$u = \frac{r_B}{r_X}$$

where r_A, r_B, and r_X are radii of corresponding ions. The τ was computed as:

$$\tau = \frac{r_X}{r_B} - n_A \times \left(n_A - \frac{\frac{r_A}{r_B}}{ln(\frac{r_A}{r_B})} \right)$$

Where n_A is the oxidation state of A. As indicated by past investigations, the scopes of the octahedral factor μ are $0.44 < \mu < 0.90$ and the tolerance factor τ is $0.81 < t < 1.11$. Also, when $\tau < 4.18$, stable perovskites are expected empirically.

Note S2 The necessity of the Hubbard U correction for 3d transition-metal

To evaluate the necessity of the Hubbard *U* correction, we performed benchmark calculations on a representative structure using the DFT+*U* method (Figure S1). The results show that although introducing *U* leads to some changes in the electronic structure near the Fermi surface, the resulting change in the migration barrier is minimal. Therefore, *U* correction does not affect our subsequent analysis of migration paths or the construction of ML regression models. Importantly, this study aims to compare halide migration in a range of different main group and transition metals. In such comparative studies, using element-specific *U* values (which are not uniquely determined) introduces additional, non-uniform degrees of freedom, thus reducing the accuracy of cross-composition comparisons. Therefore, in this study, we employ a consistent spin-polarized GGA level treatment across the entire dataset, without using *U* values, to maintain methodological consistency.

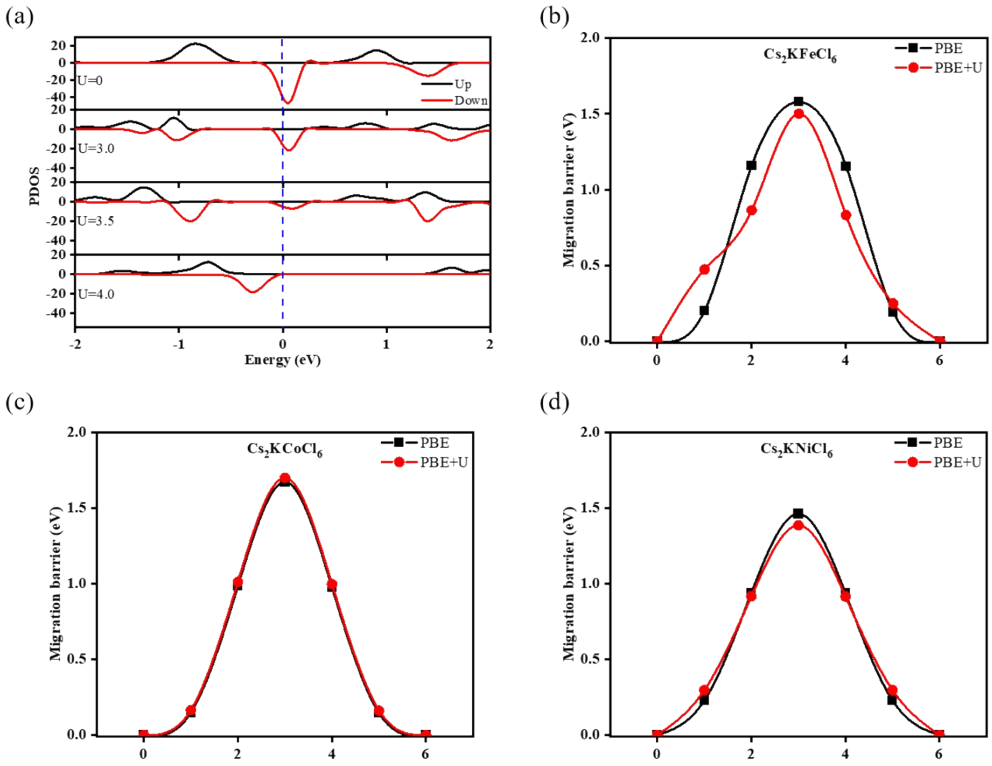

Figure S1 Effect of Hubbard *U* correction on (a) electronic structure and migration barrier for (b) Cs_2KFeCl_6, (c) Cs_2KCoCl_6, (d) Cs_2KNiCl_6

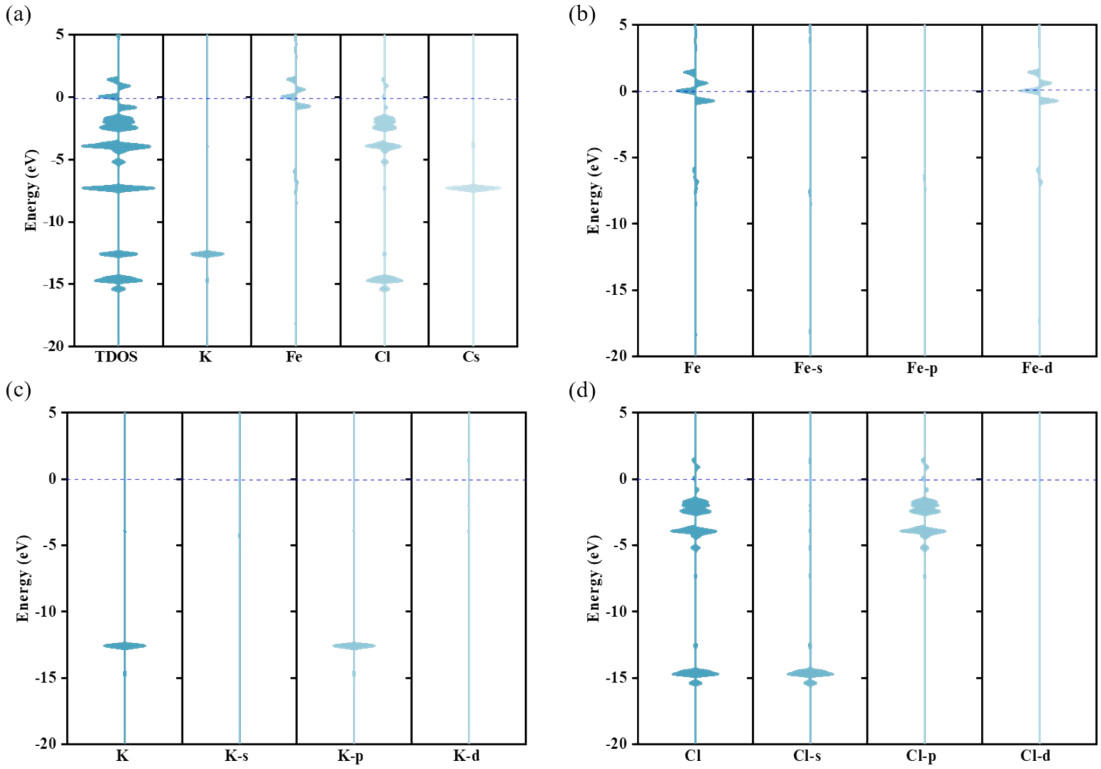

Figure S2. (a) The total density of states (TDOS) of Cs_2KFeCl_6 and Partial density of states (PDOS) of K (b), Fe (c), and Cl (d) elements.

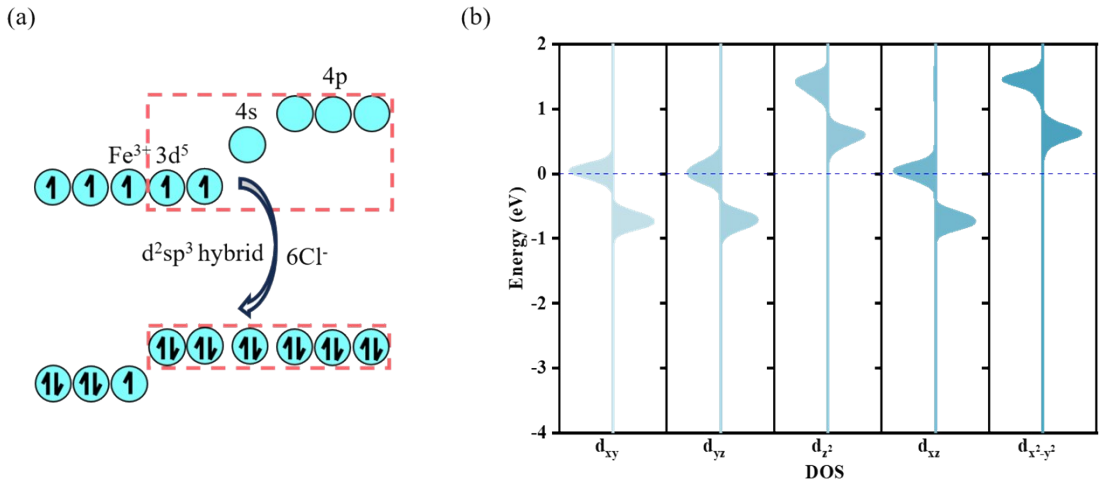

Figure S3. (a) Schematic illustration of d^2sp^3 hybridization of Fe^{3+} and Cl^- in Cs_2KFeCl_6 perovskite. (b) d orbitals density of states (DOS) of Fe^{3+}.

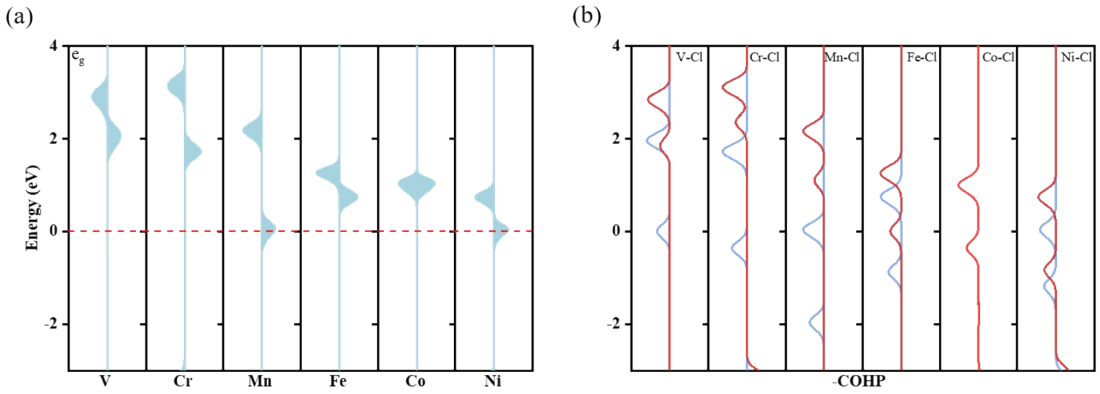

Figure S4. (a) The e_g orbital arrangement for different B_{III}-site 3d transition metals. (b) The ICOHP of B_{III}-Cl bond for different B_{III}-site 3d transition metals.

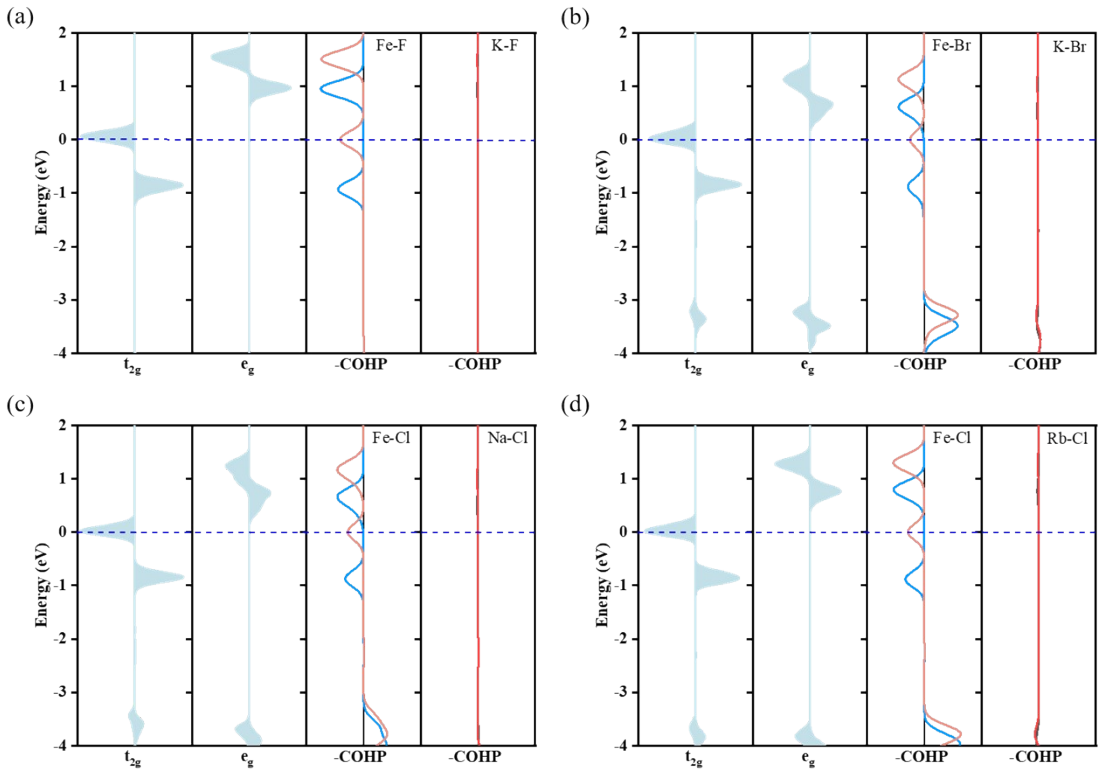

Figure S5. (a) d-DOS of Fe^{3+} and COHP of Fe-F and K-F bond in Cs_2KFeF_6 perovskite. (b) d-DOS of Fe^{3+} and COHP of Fe-Br and K-Br bond in Cs_2KFeBr_6 perovskite. (c) d-DOS of Fe^{3+} and COHP of Fe-Cl and Na-Cl bond in $Cs_2NaFeCl_6$ perovskite. (d) d-DOS of Fe^{3+} and COHP of Fe-Cl and Rb-Cl bond in $Cs_2RbFeCl_6$ perovskite.

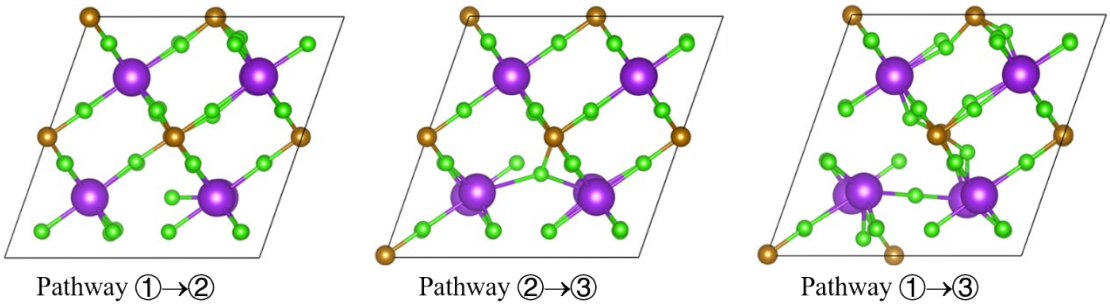

Figure S6. The lattice distortion induced by the direct transition (pathway ①→② and ②→③) and edge-mediation migration (pathway ①→③).

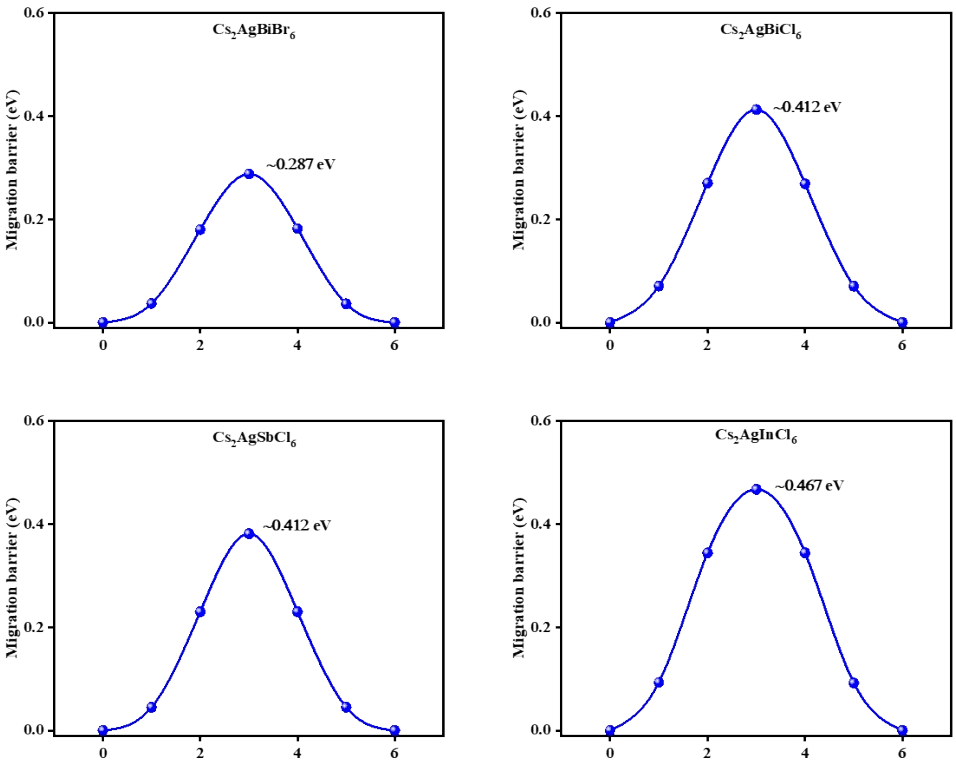

Figure S7. The migration barriers of halogen ions in Ag-based halide double perovskites.

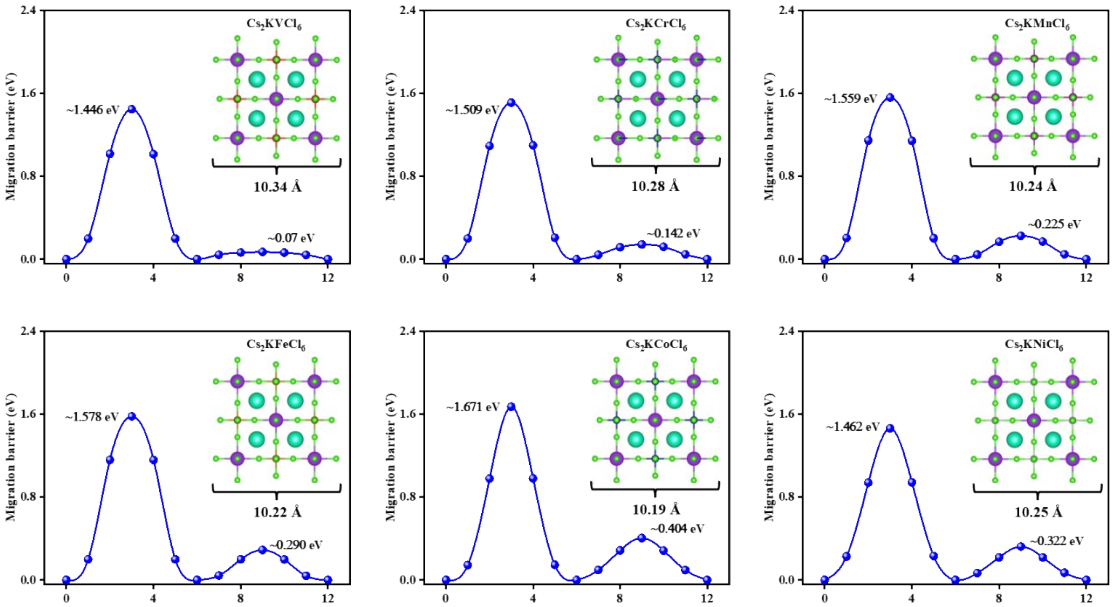

Figure S8. The migration barriers (along pathway 1) of halogen ions in double perovskites with different B_{III}-site 3d transition metals (V, Cr, Mn, Fe, Co, Ni).

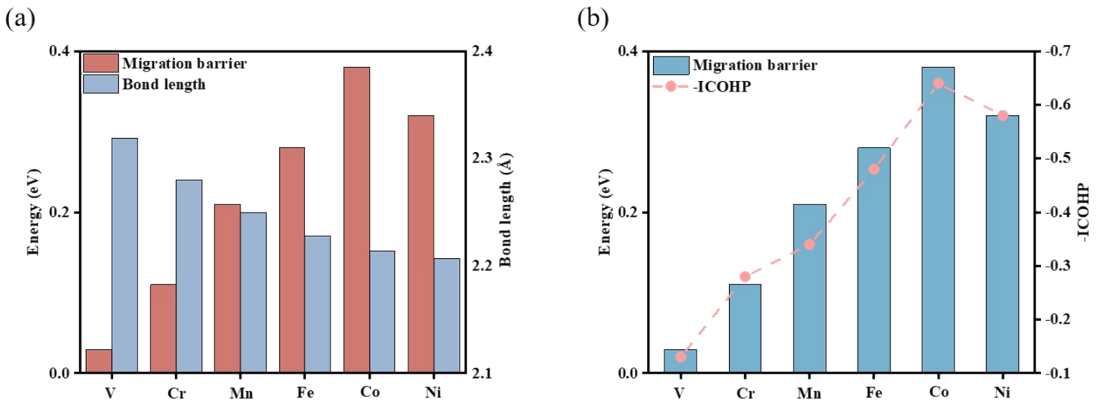

Figure S9. The bond length of the TS of B_{III}-Cl bond for different 3d transition metals. (e) The ICOHP analysis of the TS of B_{III}-Cl bond for different 3d transition metals.

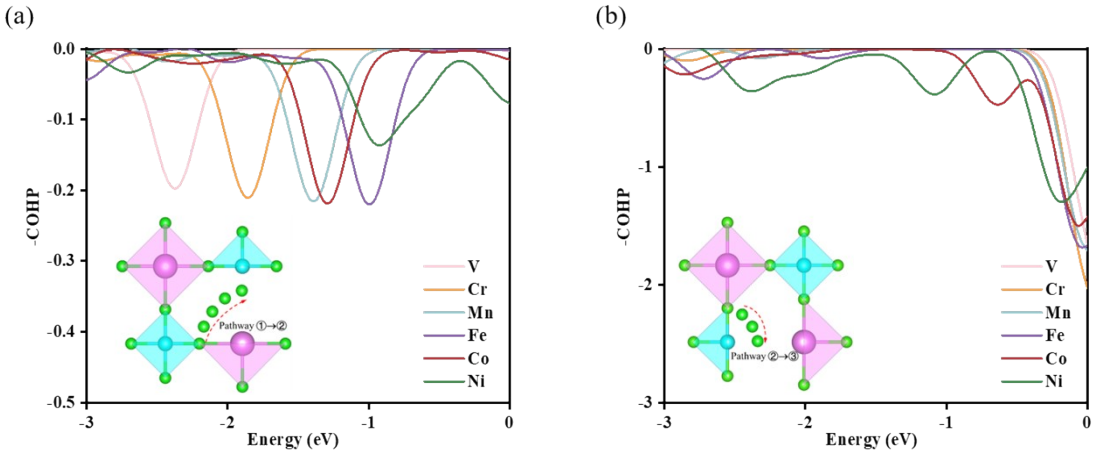

Figure S10. The COHP analysis of the (a) K-Cl and (b) B_{III}-Cl bond under the influence of different 3d transition metals.

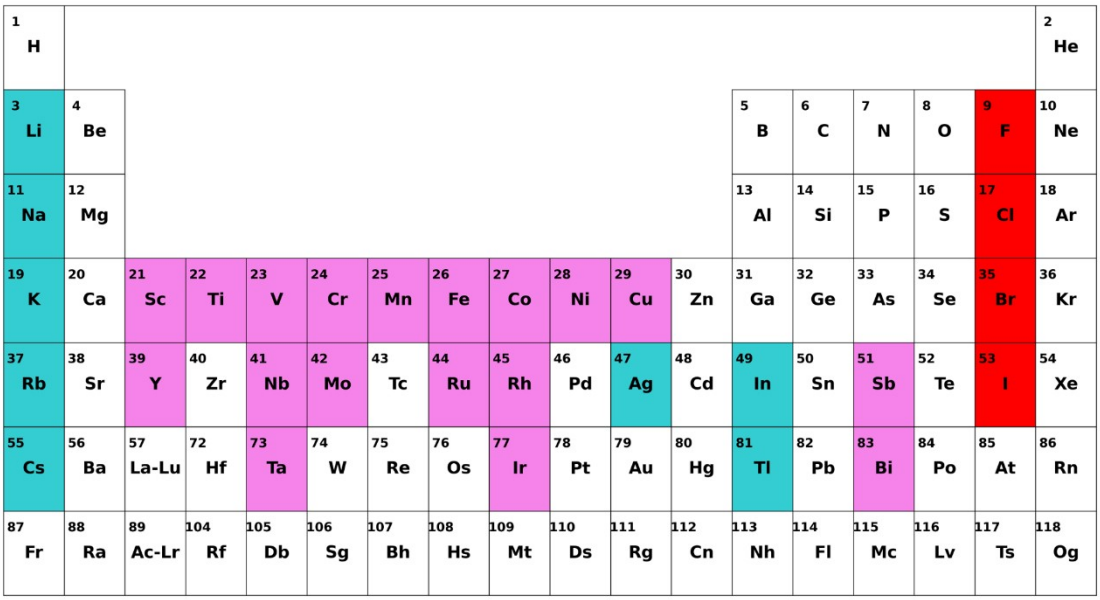

Figure S11. The potential BI (blue), BIII (pink), and X-site (red) elements selected in this study.

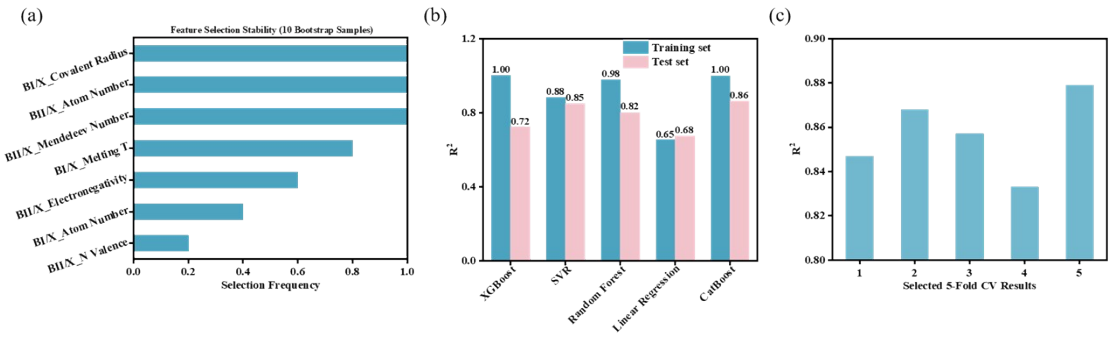

Figure S12. (a) Feature selection stability of the ML models. (b) Performance comparison of different ML models, including XGBoost, SVR, Random Forest, Linear Regression, CatBoost. (c) 5-fold cross validation results of the SVR model.

Table S1 The ΔE_f of different vacancies in Cs_2KFeCl_6 double perovskite

Defect	V_{Cs}	V_K	V_{Fe}	V_{Cl}
ΔE_f (eV)	3.76	3.48	5.96	1.93

Reference

1. N. K. Tailor, A. Listorti, S. Colella and S. Satapathi, *Adv Materials Technologies*, 2023, **8**, 2200442.